Research in Astron. Astrophys. **2012** Vol. **12** No. **5**, 584–590
http://www.raa-journal.org *http://www.iop.org/journals/raa*

Research in Astronomy and Astrophysics

Simulation and fabrication of the atmospheric turbulence phase screen based on a fractal model

Peng Jia[1,2,3,4] and Sijiong Zhang[2,3]

[1] School of Astronomy & Space Science, Nanjing University, Nanjing 210093, China
[2] National Astronomical Observatories / Nanjing Institute of Astronomical Optics & Technology, Chinese Academy of Sciences, Nanjing 210042, China; *sjzhang@niaot.ac.cn*
[3] Key Laboratory of Astronomical Optics & Technology, Nanjing Institute of Astronomical Optics & Technology, Chinese Academy of Sciences, Nanjing 210042, China
[4] Key Laboratory of Modern Astronomy and Astrophysics (Nanjing University), Ministry of Education, Nanjing 210093, China

Received 2011 November 11; accepted 2012 January 17

Abstract An atmospheric turbulence phase screen generated using a fractal method is introduced. It is etched onto fused silica and tested in the laboratory. The etched screen has relatively low cost, high resolution, and can be used in the broad waveband under severe temperature conditions. Our results are shown to agree well with the theory.

Key words: instrumentation: adaptive optics — turbulence atmospheric effects

1 INTRODUCTION

Adaptive optics systems are widely used (Beckers 1993) in modern ground-based optical-infrared telescopes. They can improve the performance of the optical signal by using information about atmospheric turbulence (Roggemann & Welsh 1996). Adaptive optics systems include many expensive instruments, and because many parameters have an effect on the system, the overall system performance evaluation is very complex. So small scale experiments on the system are very important for real system applications. These small scale experiments are often carried out after simulation of the system on a computer. The experiments model the wavefront sensor, deformable mirror, telescope and its accessories, the atmosphere and the stars, in the laboratory. The model of the atmosphere in the laboratory simulates the abberation induced by atmospheric turbulence. There are many ways to create the laboratory model of the atmosphere. Liquid crystal (Hu et al. 2006) is often used to create the atmosphere phase screen. It works in the phase modulation mode to induce the abberation of atmospheric turbulence. If we want to simulate the MCAO (Multi-conjugate Adaptive Optics) or GLAO (Ground Layer Adaptive Optics) system, we need at least four liquid crystal devices (Andersen et al. 2006) to model the different layers of the atmosphere. Because the liquid crystal device is expensive, four devices can cost a lot. Besides, liquid crystal does not have good performance in the infrared band, so we need to find another way to generate the atmosphere phase screen.

In this paper, we generate an atmosphere phase screen with our fractal method and etch it on the fused silica. The etched fused silica phase screen costs less than the liquid crystal and can also form a dynamical phase screen when it rotates. We tested the etched fused silica in the laboratory and the results show good agreement with the theory.

2 THE ATMOSPHERIC TURBULENCE FRACTAL MODEL

2.1 Atmospheric Turbulence Effects

Temperature variations cause random changes in wind velocity, and ultimately the change in temperature causes a change in density. Because the density affects the index of refraction of the atmosphere, the variation in the index of refraction of the atmosphere changes the phase of the wavefront from stars and makes the images of the stars twinkle and quiver. Kolmogorov (Tennekes & Lumley 1972) analyzed the phenomenon of turbulence in 1941 and published many results about it. This kind of turbulence satisfies the Navier-Stokes equation

$$\partial_t \boldsymbol{v} + \boldsymbol{v} \cdot \nabla \boldsymbol{v} = -\nabla p + \mu \nabla^2 \boldsymbol{v} \,, \tag{1}$$

where $\boldsymbol{v}$ is the velocity, p is the pressure and μ is the kinematic viscosity. In general, the turbulence's properties are described by Reynolds number Re. The Reynolds number is defined by

$$R = \frac{LV}{\mu} \,, \tag{2}$$

where V is the characteristic velocity, L is the characteristic scale and μ is the kinematic viscosity. The Reynolds number is an important parameter that describes the properties of turbulence. If turbulence fully develops, the Reynolds number will become very large. Atmospheric turbulence is generally viewed as fully developed turbulence with a very large Reynolds number. The atmosphere's temperature difference divides the atmosphere into many different parts (inside each part the atmospheric temperature is modeled as having the same value). The temperature gradient forces different parts to mix, and as they mix the size of each part becomes progressively smaller. If the size of the part is small enough then molecular diffusion becomes important, the turbulence development process stops and all the energy is diffused as thermal energy. Because the Navier-Stokes equation is nonlinear and very sensitive to initial conditions, the determined equation with the initial condition cannot fully describe the turbulence. In general, the atmosphere is described using a statistical method. Kolmogorov studied the mean-square velocity difference between two points in the atmosphere by the displacement vector $\boldsymbol{r}$, and introduced a structure function to describe the statistical properties. The structure function is simplified to

$$D_{ij} = \langle [v_i(\boldsymbol{r}_1 + \boldsymbol{r}) - v_i(\boldsymbol{r}_1)][v_j(\boldsymbol{r}_1 + \boldsymbol{r}) - v_j(\boldsymbol{r}_1)] \rangle \,. \tag{3}$$

The structure can be simplified if the following conditions are satisfied: the atmosphere is locally homogeneous, locally isotropic, incompressible and the separation is within the inertial scale. The inertial scale should be bigger than the inner scale (about a few millimeters) and smaller than the outer scale (tens to hundreds of meters). The structure function is described by

$$D_v = C_v^2 r^{2/3} \,. \tag{4}$$

Tatarskii (1971) related the velocity structure to the index of refraction structure and found the following results

$$D_n(r) = C_n^2 r^{2/3} \,, \tag{5}$$

where C_n is the refractive index structure constant. This is the measure of turbulence strength.

The structure function can be expressed in a simple way if we introduce the Fried parameter. The Fried parameter is the maximum diameter of a collector that is allowed before atmospheric distortion limits performance. It is defined as

$$r_0 = \left[0.423k^2 \sec(\beta) \int_0^L C_n^2(h)dh\right]^{-3/5} . \tag{6}$$

The phase structure function for the plane wave can be written as

$$D_\phi = 6.88\left(\frac{r}{r_0}\right)^{5/3} \tag{7}$$

with the Fried parameter. The phase structure function is a basis for the fractal atmospheric turbulence simulation. The Fried parameter and wind velocity are independent parameters (Roddier 1981), and they can fully describe the atmosphere. The Fried parameter is a measure of the spatial correlation. If the Taylor frozen flow assumption is satisfied, the temporal correlation can be derived with the Fried parameter and the wind velocity because, under the assumption, the turbulence is frozen and travels in the wind's direction with the wind's velocity. The Fried parameter and wind velocity are always needed for the simulation.

2.2 The Fractal Model for Atmospheric Turbulence

The atmospheric turbulence phase screen satisfies Equation (7) and also another relation. It is continuous and if the distance between two points is zero, then according to Equation (7) the structure function is zero. If we consider the phase as the height of the surface, the atmospheric turbulence phase screen can be viewed as a fractional Brownian surface (Mandelbrot 1982). According to Falconer (Falconer & Lévy Véhel 2000), the fractional Brownian surface is the surface with height that satisfies the fractional Brownian function $X\colon \mathbb{R}^2 \to \mathbb{R}$ such that it is a Gaussian random function with index α ($1>\alpha>0$) given by

(i) with probability 1, $X(0,0) = 0$, and $X(x,y)$ is a continuous function of (x,y);
(ii) for (x,y), $(h,k) \in \mathbb{R}^2$ the height increments $X(x+h,y+k)-X(x,y)$ have a normal distribution with mean zero and variance $(h^2+k^2)^\alpha = |(h,k)|^{2\alpha}$.

The definition of the fractal Brownian surface shows that the height increments of the surface are not independent, and because the atmospheric turbulence phase screen's α (Hurst parameter) is 5/6, the increments are positively related. The Hurst and Hausdorff parameters have the following relation: $F = 3 - E$, where F is the Hausdorff parameter and E is the Hurst parameter. The Hausdorff parameter is used to describe the coverage ability of the surface. If the scale reduces to λ scale, the surface should be reduced to λ^F to maintain the fractal properties. The fractal model of the atmospheric turbulence phase screen uses the existing column to extrapolate new columns based on the fractal algorithm, and the atmospheric turbulence phase screen does not only have the spatial correlation. If we use the Taylor frozen flow assumption (Hugo & Jumper 1996) and consider the wind velocity, we can also find the temporal correlation. Then the phase screen can be extrapolated along the wind velocity as time evolves (Assémat et al. 2006). The phase of the new point is calculated by

$$\boldsymbol{X}_{\text{new}} = \boldsymbol{R}_m \boldsymbol{X}_{\text{old}} + \boldsymbol{B}\boldsymbol{Z} \, , \tag{8}$$

where $\boldsymbol{X}_{\text{new}}$ is the phase of the new point, $\boldsymbol{X}_{\text{old}}$ is the points used to generate the new point, $\boldsymbol{Z}$ is a random number with each value coming from a Gaussian distribution, and $\boldsymbol{B}$ is a number defined by Equation (7) with the distance defined between the newly generated point and the previously existing points. $\boldsymbol{R}_m$ is the extrapolated parameters. Two of the extrapolated methods are shown in Figure 1. According to Schwartz (Schwartz et al. 1994), the extrapolating parameters are calculated by

$$\boldsymbol{R}_m = \boldsymbol{M}^{-1}\boldsymbol{P}\,, \tag{9}$$

where $\boldsymbol{M}^{-1}$ is the normalized distance matrix and $\boldsymbol{P}$ is the normalized distance vector. We call the points used to extrapolate the new point "cells" and the extrapolated parameters "kernels." The calculation of each kernel can be extended to more than four orders, and the cell can be extended to seven points. Some types of estimated kernels are shown in Table 1 (coordinate x is the extrapolated direction).

Table 1 The Estimated Kernel and Parameters for the Different Cells

Estimated Cells to Be Used	Estimated Kernel
$\begin{bmatrix} x-d, y \\ x-d, y \pm d \\ x-2d, y \end{bmatrix}$	$\begin{bmatrix} 0.6997 \\ 0.3703 \\ -0.4659 \end{bmatrix}$
$\begin{bmatrix} x-d, y \\ x-d, y \pm d \\ x-d, y \pm 2d \end{bmatrix}$	$\begin{bmatrix} 0.5065 \\ 0.1955 \\ 0.0513 \end{bmatrix}$
$\begin{bmatrix} x-d, y \\ x-d, y \pm d \\ x-d, y \pm 2d \end{bmatrix}$	$\begin{bmatrix} 0.5042 \\ 0.1966 \\ 0.0448 \end{bmatrix}$
$\begin{bmatrix} x-d, y \\ x-d, y \pm d \\ x-d, y \pm 2d \\ x-d, y \pm 3d \end{bmatrix}$	$\begin{bmatrix} 0.5043 \\ 0.2016 \\ 0.0248 \\ 0.0158 \end{bmatrix}$

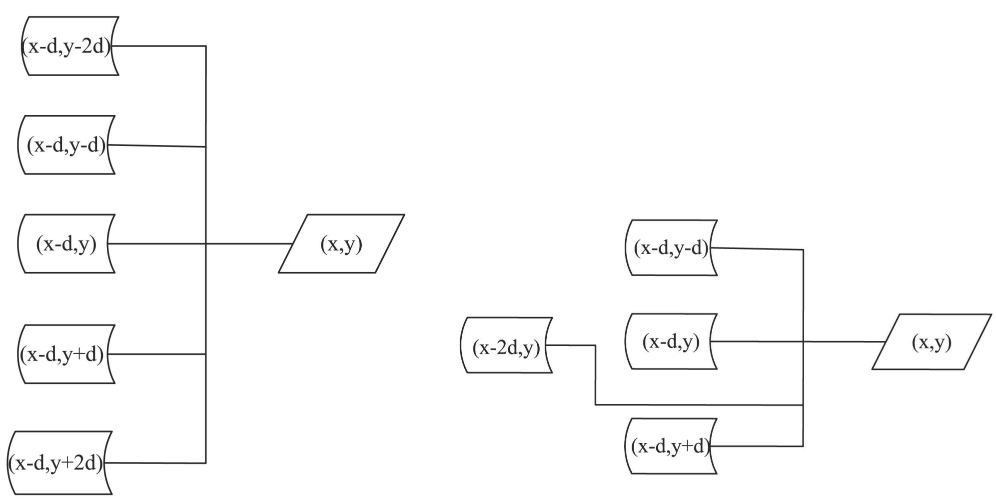

Fig. 1 Two of the methods used to generate the new point's phase value.

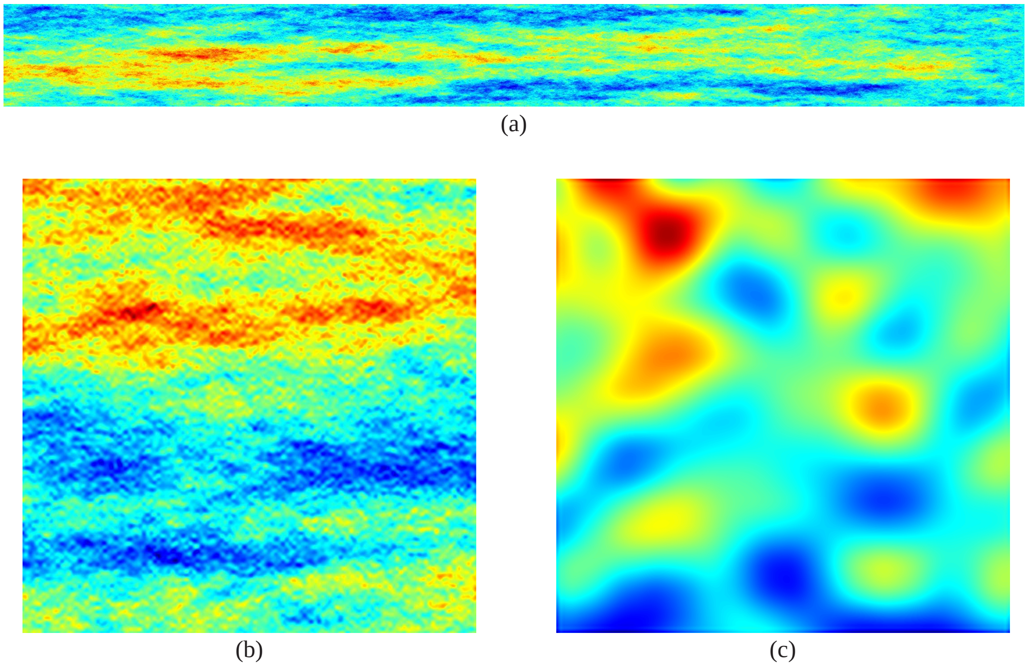

Fig. 2 (a) The main map generated in the first step; (b) the map generated by the second step; and (c) the output signal for the liquid crystal device.

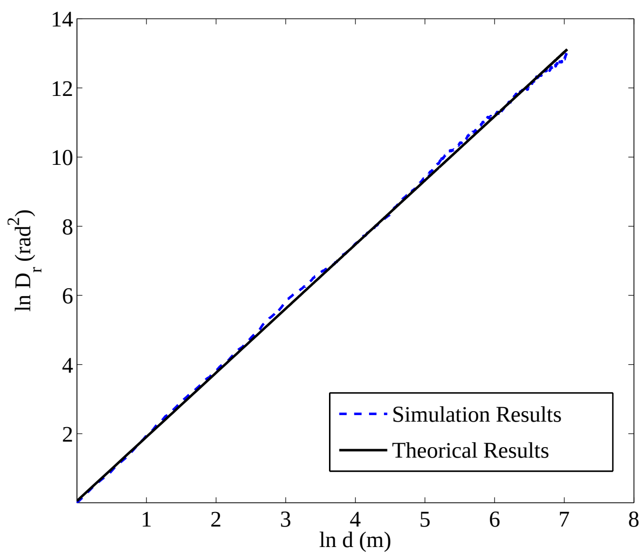

Fig. 3 Relation of structure function, D_r, and distance, d, after iteration to 4000 pixels.

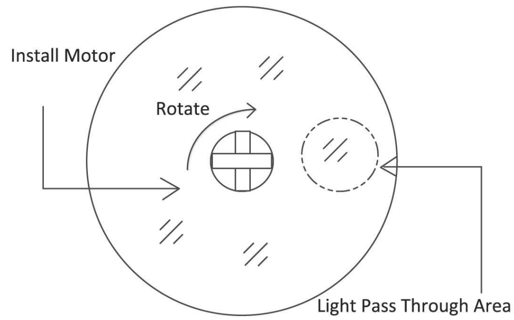

Fig. 4 The assembled method and the working area (where light passes through).

In this paper, we use three orders and seven points to generate the phase screen. The distance between pixels is set to r_0 (Fried parameter) to get a screen with enough size, and then the phase screen is interpolated using the random mid-point displacement method (Lane et al. 1992) to get a finer structure, as shown in Figure 2. In addition, the new interpolated points will also add a random value depending on the interpolation scale. The distance-variance relation can be seen in Figure 3, which shows that the fractal model of the atmospheric turbulence phase screen agrees well with the theoretical prediction.

3 THE FABRICATION OF THE ETCHED FUSED SILICA PHASE SCREEN

The fused silica has a high transmittance from 0.5 to $2.5\ \mu\mathrm{m}$, and a very low index of refraction change versus wavelength. The fused silica etch method is mature in the semi-conductor industry, and the etch machine can directly etch the atmospheric turbulence phase screen to the fused silica disk. When the light passes through the fused silica phase screen, the phase difference is generated by the optical path difference between different parts of the fused silica. The etch depth and the phase screen to be generated have the relation

$$\phi = (n-1)D/\lambda\,, \tag{10}$$

where ϕ is the phase difference of the wavefront, n is the refraction of the fused silica, D is the etch depth and the index of refraction of air is assumed to be 1, and λ is the wavelength of the light used in the system. We chiseled a hole in the middle of the fused silica disk and installed an axis through the hole. The axis is attached to an electrical motor. The rotation speed of the electrical motor is defined by the wind velocity and the simulation scale. When the fused silica phase screen is operating under working conditions, the beam is transmitted through part of the fused silica disk, and when the motor starts rotating, a dynamical atmospheric turbulence phase screen is obtained. Although the wind velocity has a little difference because of the different radii, this is not important in practical application. Figure 4 shows the assembly and the working methods.

4 EXPERIMENTAL RESULTS AND DISCUSSION

The fused silica atmospheric turbulence phase screen is tested in the laboratory with the following light path map as shown in Figure 4. We simulate a 2.16 m telescope with atmospheric condition $r_0 = 20\ \mathrm{cm}$ and wind velocity 6 m s^{-1} (the wind velocity can be adjusted by adjusting the rotation speed of the motor). The radius of the telescope model is reduced to 25 mm, and the fused silica atmospheric turbulence phase screen r_0 is reduced to 0.0057 cm (the scale should be reduced

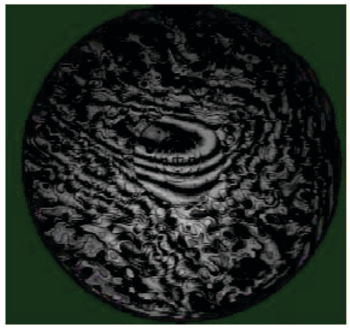

Fig. 5 Interferometry image of the phase screen etched onto the fused silica.

considering the Hausdorff measure) to match the telescope size as shown in

$$r_{0c} = \frac{r_0}{\left[D_{\rm tel}/(2 \times r_{\rm tel})\right]^{13/6}}\,, \tag{11}$$

where $13/6$ is the Hausdorff parameter, r_{0c} is the Fried parameter in the fused silica atmospheric turbulence phase screen, r_0 is $20\ \mathrm{cm}$, $D_{\rm tel}$ is the diameter of the 2.16 m telescope and $r_{\rm tel}$ is the radius of the telescope model. The phase screens are tested in the Wyko interferometer, and the test results are shown in Figure 5. The results show that the phase screen has indeed been etched on the surface.

From the results, it can be seen that the fractal atmosphere phase screen etched on the fused silica can model the atmospheric turbulence phase screen in the laboratory with good performance in a broad band. It also costs less than the liquid crystal device. Because the optical properties of the fused silica are not very sensitive to temperature, they can be further used in the telescope dome to calibrate the correction ability of the adaptive optics system, but the liquid crystal cannot (the telescope dome's temperature is always less than the working temperature of the liquid crystal).

Acknowledgements Many thanks to Changwei Li's great help in the simulation set up, and Bangming Li's helpful discussion. This work is supported by the dedicated operation funding for astronomical observation stations and facilities from the Chinese Academy of Sciences.

References

Andersen, D. R., Stoesz, J., Morris, S., et al. 2006, PASP, 118, 1574
Assémat, F., Wilson, R., & Gendron, E. 2006, Optics Express, 14, 988
Beckers, J. M. 1993, ARA&A, 31, 13
Falconer, K. J., & Lévy Véhel, J. 2000, Royal Society of London Proceedings Series A, 456, 2153
Hu, L., Xuan, L., Cao, Z., et al. 2006, Optics Express, 14, 11911
Hugo, R. J., & Jumper, E. J. 1996, Appl. Opt., 35, 4436
Lane, R. G., Glindemann, A., & Dainty, J. C. 1992, Waves in Random Media, 2, 209
Mandelbrot, B. B. 1982, The Fractal Geometry of Nature (San Francisco, CA: Freema)
Roddier, F. 1981, in Progress in Optics (Amsterdam: North-Holland Publishing Co.), 19, 281
Roggemann, M. C., & Welsh, B. 1996, Imaging through Turbulence (CRC Press)
Schwartz, C., Baum, G., & Ribak, E. N. 1994, Journal of the Optical Society of America A, 11, 444
Tatarskii, V. I. 1971, The Effects of the Turbulent Atmosphere on Wave Propagation, Jerusalem: Israel Program for Scientific Translations
Tennekes, H., & Lumley, J. L. 1972, First Course in Turbulence (Cambridge: MIT Press)